Neurochemistry International 129 (2019) 104507

Contents lists available at ScienceDirect

Neurochemistry International

journal homepage: www.elsevier.com/locate/neuint

Phytic acid attenuates upregulation of GSK-3β and disturbance of synaptic vesicle recycling in MPTP-induced Parkinson's disease models

Liping Wang[a], Zheng Zhang[a,*], Lin Hou[a,**], YueHua Wang[a], JinHui Zuo[a], MeiLan Xue[a], XiangHong Li[b], YongChao Liu[c], JinLian Song[d], FengYu Pan[e], TingWei Pu[e]

[a] Biochemistry and Molecular Biology Department of Preclinical Medicine College, Qingdao University. NO.308 Ningxia Road. Qingdao, Shandong, 266071, China
[b] Department of Neonatology, The Affiliated Hospital of Qingdao University, No.16 Jiangsu Road, Qingdao, Shandong 266000, China
[c] Department of Immunology, Beihua University, Binjiang East Road 3999. Jilin, Jilin, 132013, China
[d] Department of Laboratory, The Affiliated Women and Chidlldren's Hospital of Qingdao University. Qingdao, Shandong, 266071, China
[e] Undergraduate of Qingdao University. NO.308 Ningxia Road. Qingdao, Shandong, 266071, China

A B S T R A C T

Heightened activity of glycogen synthase kinase-3β (GSK-3β) is linked to the degeneration of dopaminergic neurons in Parkinson's disease (PD). Phytic acid (PA), a naturally occurring compound with potent antioxidant property, has been shown to confer neuroprotection on dopaminergic neurons in PD. However, the underlying mechanism remains unclear. In the present study, MPTP and MPP^+ treatments were used to model PD in mice and SH-SY5Y cells, respectively. We observed reduced tissue dopamine, disrupted synaptic vesicle recycling, and defective neurotransmitter exocytosis. Furthermore, expression of GSK-3β was upregulated while that of β-catenin was downregulated, concentration of cytosolic calcium was increased, and expressions of two dopamine carriers, dopamine transporter (DAT) and vesicular monoamine transporter 2 (VMAT2) were decreased. PA treatment attenuated the MPTP-induced upregulation of GSK-3β, increase in cytosolic calcium concentration, decreases in the levels of DAT, VMAT2, tissue dopamine, and synaptic vesicle recycling. Importantly, disturbances in synaptic vesicle recycling are thought to be early events in PD pathology. These findings suggest that PA is a promising therapeutic agent to treat early events in PD.

1. Introduction

GSK-3β is recently reported to be a multifunctional mediator of several cellular biological processes, and therefore, pharmacological inhibitors of GSK-3β have great therapeutic potentials for many disorders (Chen et al., 2007; Zhang et al., 2016a; Leikas et al., 2017). Considerable research has shown that GSK-3β participates in synaptic maintenance and plays a crucial role in synaptic physiology (Bradley et al., 2012). Inhibition of GSK-3β is reported to favor synaptic homeostasis and regulate dopamine actions in vivo. Upregulation of GSK-3β markedly inhibits presynaptic glutamate release and synaptic vesicle protein expression. Thus, inhibition of GSK-3β attenuates reduction of presynaptic transmission and interrupted SNARE complex formation (Zhu et al., 2010).

Growing evidence links disturbance of synaptic vesicle recycling with the early pathology of Parkinson's disease (PD) (Garcia et al., 2010). Neurotransmitters are released by synaptic vesicle exocytosis at presynaptic nerve terminals. Each nerve terminal contains large amounts of synaptic vesicles. After an action potential occurs, Ca^{2+}-channels open and calcium ions enter into the nerve terminal to induce neurotransmitter release (Marland et al., 2016). Disturbance in synaptic vesicle recycling interrupts the neurotransmitter release and neural dopamine homeostasis (Choi et al., 2015).

Both DAT and VMAT2 are dopamine carriers (Lohr et al., 2014). DAT is responsible for transporting dopamine from the extracellular gap into the cytoplasm of presynaptic terminal. VMAT2 is a carrier that

Abbreviations: PD, parkinson's disease; MPTP, 1-methyl-4-phenyl-1,2,3,6-tetrahydropyridine; MPP+, 1-methyl-4-phenylpyridinium ion; PA, phytic acid; DAT, dopamine transporter; VMAT2, vesicular monoamine transporter 2; SNARE, soluble N-ethylmaleimide sensitive fusion attachment protein receptor; MTT, 3-(4, 5-Dimethythiazol-2-yl)-2, 5-diphenyl tetrazolium bromide; TH, tyrosine hydroxylase; HPLC, high-performance liquid chromatography; DA, dopamine; DOPAC, 3,4-dihydroxyphenylacetic acid; HVA, homovanillic acid; OD, Optical density; ANOVA, one-way analysis of variance

* Corresponding author.
** Corresponding author.
E-mail addresses: qdzenobiazz@163.com (Z. Zhang), linhou@qdu.edu.cn (L. Hou).

https://doi.org/10.1016/j.neuint.2019.104507
Received 16 March 2019; Received in revised form 14 July 2019; Accepted 16 July 2019
Available online 17 July 2019
0197-0186/

packages cytosolic dopamine into vesicular compartments for subsequent neurotransmitter release. Taken together, DAT and VMAT2 maintain the balance of synaptic vesicle recycling in synaptic terminals (Avelar et al., 2013).

PA is widely distributed in animal and plant cells. It serves as a multifaceted player in several signaling pathways (Mackenzie et al., 2016). Studies have shown that PA crosses the blood-brain barrier and exists as 10 times the concentration in brain tissues relative to other tissues (Grases et al., 2001). As a bivalent metal ion chelator Fig. 1, PA has potent antioxidant property and confers neuroprotection on dopaminergic neurons in PD (Zhang et al., 2016b).

In the preliminary study, we found PA remarkably inhibited GSK-3β upregulation induced by MPP^+. Consequently, we used dopaminergic neurons treated with MPTP or MPP^+ to induce PD models, observed levels of tissue dopamine and synaptic vesicle recycling with or without PA treatment. Expressions of DAT, VMAT-2, β-catenin and calcium level were detected to determine the mechanism involved in PA's effect on synaptic vesicle recycling.

2. Materials and methods

2.1. Animals and treatment

C57/BL6 mice (8 weeks old, 20–22 g) were obtained from the Animal Center of Shandong Institute of Drug Control. Animals were housed in a standard environment with controlled temperature and humidity condition. After arrival, mice were given 6 d to acclimate before drug administration. PD mice were prepared as shown in Fig. 2A. Doses of PA were prepared according to our previous study (Lv et al., 2015). All procedures were performed in compliance with the National Institutes of Health Guide for the Care and Use of Laboratory Animals, and were approved by the Animal Ethics Committee of Qingdao University. All efforts were made to minimize animal suffering.

2.2. Cell culture and treatment

The human neuroblastoma cell line, SH-SY5Y, was maintained in minimal essential media (MEM) supplemented with heat-inactivated newborn calf serum (10%, v/v), penicillin (100 IU/ml), and streptomycin (100 μ g/ml) in humidified 5% CO_2/95% air at 37 °C. Cells were cultured at the density of 2×10^5 cells/ml on 96-well plates. Phytic acid (PA) groups or MPP^+ group: cells were pretreated with PA (50, 150, 300 μ M) or saline for 24 h and then subjected to 1 mM MPP^+ for 12 h. SALINE group: cells were treated with saline for 24 h and then exposed to saline for 12 h. After incubation, cells were harvested for immunofluorescence analysis or activity assays. Proteins from cell lysates were detected by Western blot analysis.

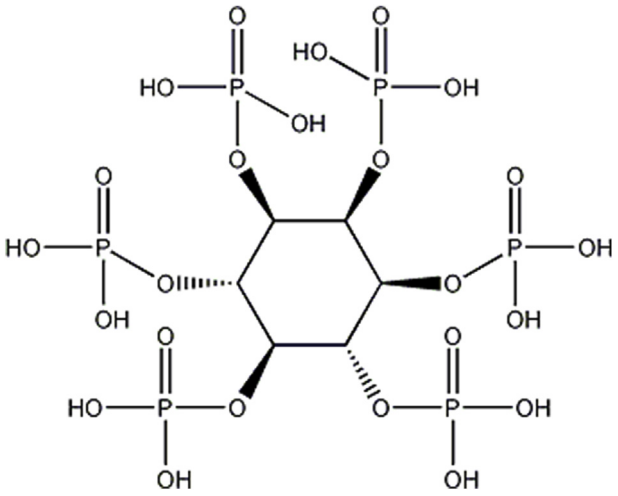

Fig. 1. Molecular formula of phytic acid (PA).

2.3. Cell viability assay

The 3-(4, 5-Dimethythiazol-2-yl)-2, 5-diphenyl tetrazolium bromide (MTT) assay was used to assess cell viability (Wang et al., 2017). Following MPP^+ exposure, cells were incubated with MTT reagent (0.1 mg/ml) in 0.5% serum-containing medium at 37 °C for 1 h. Formazan crystals were precipitated by centrifugation at 1900 × *g*. Next, medium was aspirated and then the crystals were dissolved in dimethyl sulfoxide (DMSO). The optical density was read at 570 nm, and group values were compared with that of saline group set to 100%.

2.4. Immunohistochemical staining and immunofluorescent staining

Brains were removed and fixed in 4% paraformaldehyde for 6 h, then, transferred to 30% sucrose until sectioning. Sections (20 μ m) were cut on a freezing microtome (Leica, Wetzlar, Hesse-Darmstadt, Germany). Alternate SN sections were stained for TH. After being washed three times in phosphate buffer saline (PBS) plus 0.3% Triton X-100, sections were incubated overnight with primary antibody of rabbit anti-TH (TH; 1:1000; Sigma, St Louis, MO, USA) overnight at 4 °C; The secondary antibody used was goat biotinylated anti-rabbit IgG (Vector, USA). To verify the immune specificity, control sections were processed with the same protocol, except that omitting the primary antibody. MBF Stereo Investigator software (MBF Bioscience) was applied to estimate the numbers of TH-positive neurons in the SN (Jia et al., 2018). One of every six serial sections was selected for counting neuron numbers to cover the entire mouse brain. Stereological details were as follows: counting grid, 240 μ m × 180 μ m; counting frames, 80 μ m × 60 μ m.

Sections for Immunofluorescent staining were fixed in 4% paraformaldehyde for 10 min followed by washing three times with PBS (Diao et al., 2017). Blocking with 5% goat serum for 1 h, sections were incubated with anti-synap-25 (all diluted 1:250; Cell signaling technology, USA) overnight at 4 °C. Washing with PBS three times, sections were incubated with fluorescent conjugated secondary antibodies (1: 1000, Cell signaling technology, USA) for 2 h. After washing with PBS, sections were treated with nuclear stain DAPI (40,6-diamidino-2-phenylindole) (Sigma, St Louis, MO, USA) for 20 min. Photomicrographs were taken with a camera linked to a fluorescence microscope (Olympus, Japan).

2.4.1. Rotarod test

Motor activity of mice was measured by rotarod test using an instrument with a 3 cm accelerated Rota-Rod (Rockenstein et al., 2014). The rotarod system included start speed, acceleration and highest speed. Mice were allowed to acclimatize for 20 s at the start speed (4 rpm) and then the rotor was gradually accelerated to the highest speed of 40 rpm during a period of 5 min. Fall of the animal from the rod was taken as the end point of test. Each animal was tested three times each day with an hour of rest between consecutive runs. Animals were tested at the 1st, 2nd, 3rd, 4th, and 7th day after the final MPTP treatment.

2.5. Dopamine release

Striatal tissue was homogenized in 200 μ l of 0.1 N perchloric acid (Sigma, St Louis, MO, USA) and centrifuged at 12,000 × *g* for 10 min at 4 °C. HPLC with electrochemical detection was applied to evaluate levels of dopamine (DA), 3,4-dihydroxyphenylacetic acid (DOPAC) and homovanillic acid (HVA) (Sigma, St Louis, MO, USA) in striatal supernatants, as previously described (Jensen et al., 2017). Briefly, 50 μ l supernatant was injected into the column consisting of a Waters 717 plus autosampler automatic injector, a Waters 1525 binary pump equipped with an Atlantis dC18 column and a Waters 2465

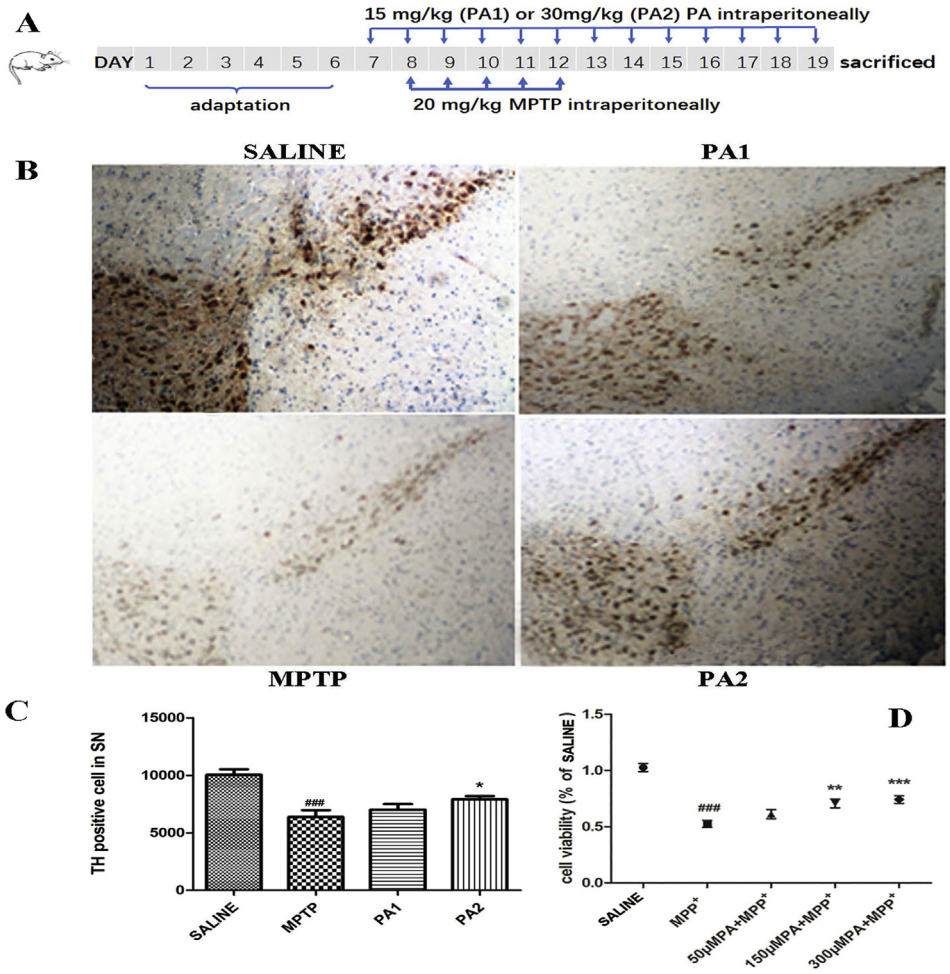

Fig. 2. Neuroprotection of PA on dopaminergic neurons in Parkinson's Disease (PD) mice and cell models. (A) Animal model preparation: Groups were prepared as follows: MPTP group: mice were injected with MPTP (20 mg/kg, intraperitoneally [I. p.]) for 5 consecutive days and were then sacrificed on day 19. n = 9; SALINE group: mice were injected with saline (20 mg/kg I. p.) for 5 consecutive days and were then sacrificed on day 19. n = 9; PA1 or PA2 groups: prior to MPTP injection, mice were pretreated with 15 or 30 mg/kg PA, respectively, I. p. daily from days 7–19. n = 9. (B) Mouse TH^+ neurons in the substantia nigra (SN) were stained using immunochemistry. TH^+ cells indicated the viability of remaining dopaminergic neurons in the nigrostriatal tissues of mouse brains. Scale bar = 20 μ m. (C) Comparison of the numbers of TH^+ cells in the SN between groups. n = 6. (D) Cell viability was measured by MTT assay in SH-SY5Y cells. Values are expressed as mean ± SEM. $^{###}p < 0.001$ compared to SALINE, $^{*}p < 0.05$ compared to MPTP, $^{**}p < 0.01$ compared to MPTP, $^{***}p < 0.001$ compared to MPTP. n = 8.

electrochemical detector. Protein levels in tissue homogenates were measured using BCA protein assay kit (Sigma, St Louis, MO, USA). Data was normalized to protein concentration and expressed in ng/mg protein.

2.6. Electron microscopy

After embedding, striatal tissue of mice brain was cut into 70 nm sections and stained with uranyl acetate and lead citrate (Rockenstein et al., 2014). Sections were imaged at × 15,000 using a JEOL JEM-1400 transmission electron microscope to see synaptic vesicles in neuron terminals.

2.7. Retention of FM1-43

SH-SY5Y cells were cultured in 24-well plates with cover slips inserted inside the wells. Treated with PA and MPP^+, cells were rinsed with Hank's balanced salts. K^+ depolarizing solution (Hank's balanced salts medium with Ca^{2+} and Mg^{2+} plus 90 mM KCL and 63 mM NaCl) was added into FM1-43 for dilution (Williams et al., 2016). Cells were incubated with 15 mM FM1-43 for 90 s at room temperature. Unbound probes were removed by washing the cells with Hanks' balanced salts medium. Fixed with 4% paraformaldehyde for 40 min, cleaned with Hanks' balanced salts medium, cells were incubated with DAPI for nuclear stain. Coverslips were sealed with 30% glycerol. Fluorescence was measured by Laser confocal microscope using excitation at 480 nm and measuring emission at 625 nm. Samples were expressed as "% fluorescence" where 100% fluorescence was defined as the amount of fluorescence in saline synaptosomes.

2.8. Intracellular free Ca^{2+} assay

Fura-2 was used to assess intracellular free Ca^{2+} in cells (Wang et al., 2015). After 12 h of MPP^+ exposure, cells were washed, suspended in Hank's balanced buffer solution (HBBS) and counted on a hemocytometer. Equal number of cells (1×10^6 cells/ml) was loaded with the fluoroprobe Fura-2 AM (invitrogen, USA) 1.5 mL at 37 °C for 40 min. Cells were washed twice with ice-cold buffer. Minimal and maximal fluorescence were detected for calculation. Concentration of $[Ca^{2+}]i$ was calculated using the equation $[Ca^{2+}]i = K_d(R - R_{min})/(R_{max} - R)$. Maximal ($R_{max}$) and minimal ($R_{min}$) ratios were determined using 25 μM digitonin and 5 mM EGTA, respectively. Percent of $[Ca^{2+}]i$ increase in exposed cells compared to saline was plotted.

2.9. Western blot assay

Immunoblotting was performed as described previously (Ma et al., 2015). Tissue or cells were harvested and lysed in cell lysis buffer for 30 min at ice and 10,000 × *g* centrifugation for 5 min. Protein concentration was adjusted to a concentration of 1.5 mg/ml with 1:1 v/v mix of homogenizing buffer and sample buffer containing 0.01% bromophenol blue. Boiled for 5 min, protein samples were concentrated and separated in 5% and 10% precast sodium dodecyl sulfate–polyacrylamide gel (Sigma, St Louis, MO, USA) at 100 V for 1 h or 1 and 1/2 h, respectively. After proteins were transferred to the Immobilon™-polyvinylidene fluoride microporous membranes (BIO-AD, USA), membranes were blocked with 5% bovine serum albumin (BSA) for 2 h. Following overnight incubation at 4 °C with appropriate primary antibodies, blots were incubated with goat-anti-rabbit conjugated

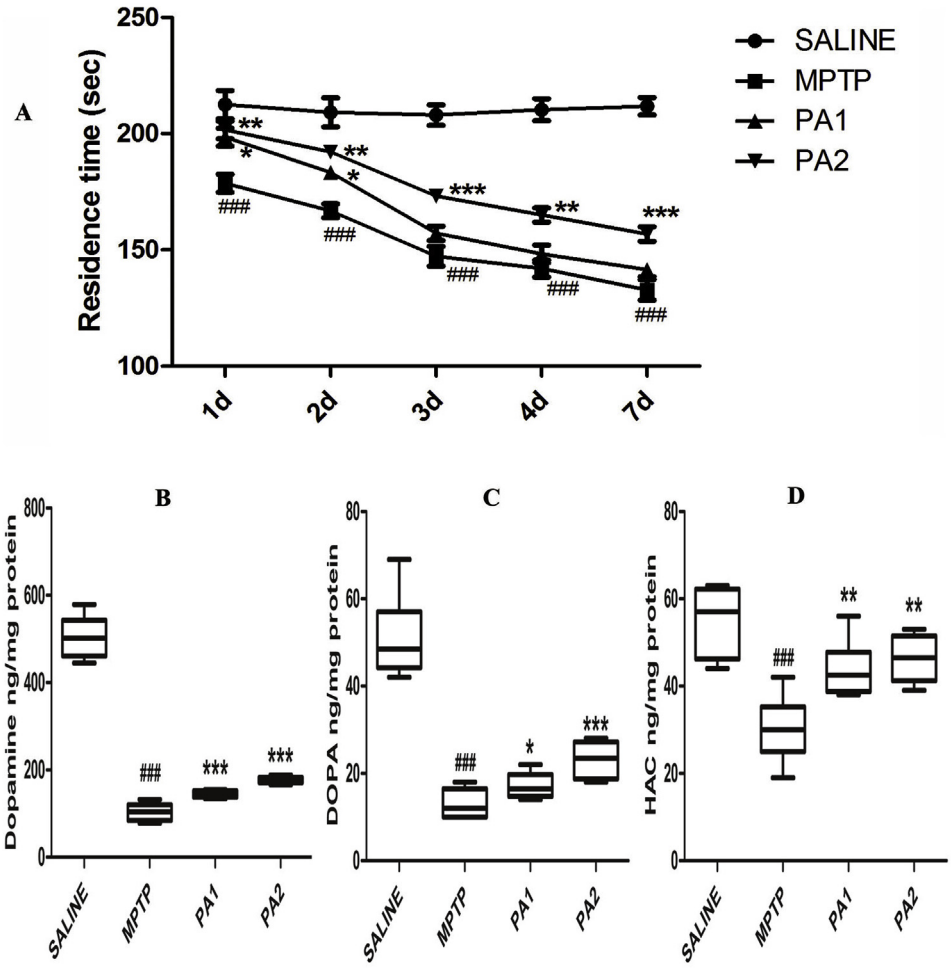

Fig. 3. PA reverses motor defects and the reduced dopamine release in PD mice. (A) The effect of PA on MPTP-induced motor deficits in mice was measured using the rotarod test. Residence time was measured on days 1, 2, 3, 4, and 7 after the last MPTP injection. Dopamine and its metabolites, 3,4-dihydroxyphenylacetic acid (DOPAC) and homovanillic acid (HVA), were assessed by high-performance liquid chromatography (HPLC), and the values are shown in (B), (C), and (D), respectively. Values are expressed as mean ± SEM. $^{###}p < 0.001$ compared to SALINE, $^{*}p < 0.05$ compared to MPTP, $^{**}p < 0.01$ compared to MPTP, $^{***}p < 0.001$ compared to MPTP. n = 6.

peroxidase secondary IgG antibodies at room temperature. Between incubations, membranes were washed 3 × 5 min in Tris–HCl buffer. Immunoreactive protein bands were detected with chemiluminescent reagent (BIO-AD, USA); images were acquired using automatic chemiluminescence image analysis system.

Antibodies used in the study included rabbit polyclonal anti-DAT, anti-VMAT2, anti-GSK-3β, anti-β-catenin (all diluted 1: 250; Cell signaling technology, USA); the bound antibodies were visualized by corresponding peroxidase-conjugated IgG antibodies (1: 1000; Sigma, St Louis, MO, USA).

2.10. Statistical analysis

Each assay was performed in duplicate and the experiment was repeated twice. Results were compared by using one-way analysis of variance (ANOVA) with Fisher's protected least significant difference (PLSD) post hoc test at 95% confidence interval. Statistical analyses were carried out with the GraphPad Prism software version 5. Data was expressed as mean ± SEM (n ≥ 3). The difference was considered significant as $p \leq 0.05$.

3. Results

3.1. Neuroprotection of PA on dopaminergic neurons in PD mice and cell models

Slices of mouse brain tissue were prepared for immunohistochemical staining of TH. Results revealed that the number of TH + neurons in the substantia nigra decreased by approximately 50% in the MPTP-damaged group. With PA treatment, the number of TH + neurons increased which suggested PA's protection on neurons in the substantia nigra ($p < 0.01$, Fig. 2B,C). Consistent with the results in vivo, PA pretreatment also conferred protection on TH + neurons in vitro. As TH + neurons, SH-SY5Y neurons had decreased cell viability exposed to 1 mM MPP^+. However, treated with PA, the number of viable cells increased significantly in a dose-dependent manner ($p < 0.01$, Fig. 2D).

3.2. PA reduces motor deficits and loss of dopamine release in MPTP-treated mice

The rotarod test was used to measure mouse balancing ability. In Fig. 3A, residence time was detected at the 1st, 2nd, 3rd, 4th, and 7th day after the last MPTP injection. We observed that MPTP-treated mice had less balancing ability relative to saline-treated animals (Fig. 3A). Moreover, motor deficits became worse with time in the MPTP group. Alternatively, treatment with 30 mg/kg PA significantly attenuated the decrease of this behavior balance ability.

Motor deficits of mice suggested dopamine defects in brain. Deficient dopamine release is an important aspect of PD pathology. Specifically, attenuated dopamine release underlies the motor deficits associated with PD. Here, we used reverse phase high-performance liquid chromatography-electrochemical detection (HPLC-ECD) to quantify dopamine and its metabolites, 3,4-dihydroxyphenylacetic acid (DOPAC) and homovanillic acid (HVA), in the mouse corpus striatum (Fig. 3B–D). Levels of dopamine, DOPAC, and HVA remarkably decreased in the MPTP group ($p < 0.001$). Alternatively, PA treatment at several doses significantly enhanced dopamine release. Results of

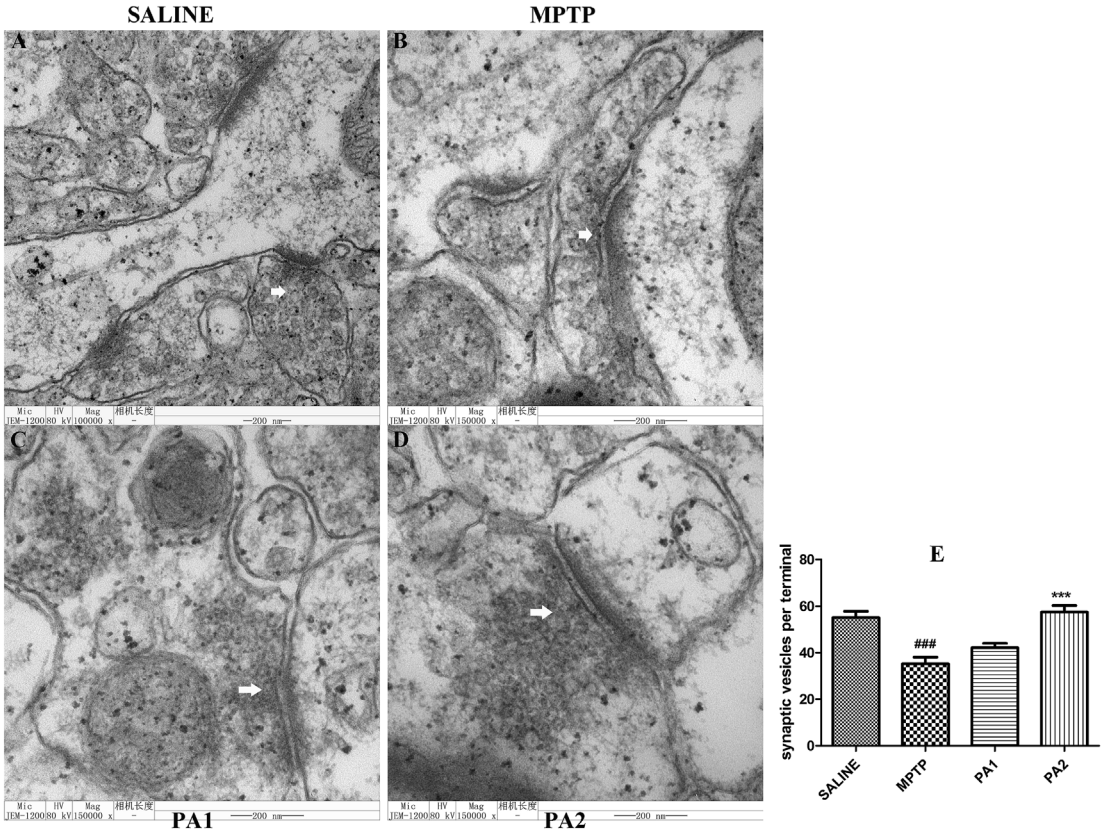

Fig. 4. PA attenuates the reduction in synaptic vesicles as shown using electron microscopy. The ultrastructure of synaptic terminals in the nigrostriatal tissues of mouse brains was visualized using electron microscopy. Representative electron micrographs are included comparing the characteristics of neuronal presynaptic terminals between groups. Arrows indicate synaptic vesicles at terminals. Scale bar = 200 nm n = 6. (A) SALINE, (B) MPTP, (C) PA1, and (D) PA2. (E) Quantification of synaptic vesicles per terminal for each group. Values are expressed as mean ± SEM. $^{###}p < 0.001$ compared to SALINE, $^{***}p < 0.001$ compared to MPTP. n = 6.

DOPAC and HVA corresponded with those of dopamine ($p < 0.001$).

3.3. PA attenuates disrupted synaptic vesicle recycling and reduced neurotransmitter exocytosis in PD models

Disturbance in synaptic vesicle recycling is thought to be an early event in PD pathogenesis, preceding neuronal degeneration (Bridi et al., 2018). In our study, electron microscopy was applied to visualize synaptic vesicles in synaptic terminals of the substantia nigra. The results revealed that numbers of synaptic vesicles in nerve terminals decreased after MPTP treatment (Fig. 4B). This suggested that MPTP reduced the formation of synaptic vesicles, and in turn, affected synaptic vesicle recycling. However, PA treatment limited this MPTP-induced reduction in vesicle number, and this improvement was significant in the PA2 group.

Synaptic vesicles are composed of SNARE complexes. Vesicles accumulation also confirmed that SNARE proteins accumulated in synaptic nerve terminals. Using immunofluorescent staining to visualize SNAP-25, one of major SNARE proteins, we assessed the expression of SNAP-25 in each group (Fig. 5). The level of SNAP-25 was consistent with the result of electron microscopy detection, MPTP treatment decreased the expression of SNAP-25, and PA treatment significantly rescued the reduced level of SNAP-25 ($p < 0.001$).

In the MPP^+-induced neuron damaged models, we used the fluorescent dye, FM1-43, to visualize neurotransmitter release and synaptic vesicle recycling by confocal microscopy (Fig. 6). Potassium ions were applied to stimulate neurotransmitter release and synaptic vesicle exocytosis. From the result we can see, less fluorescence intensity in MPP^+ treatment group indicated fewer synaptic vesicles and deficient synaptic vesicle recycling. However, PA treatment remarkably improved deficits in synaptic vesicle recycling in a dose-dependent manner ($p < 0.001$).

3.4. PA reverses MPTP/MPP^+-induced reductions in DAT and VMAT2 expression

DAT carries dopamine from the extracellular space into the cytoplasm of synaptic terminal (Blanco et al., 2018), while VMAT2 transports cytosolic dopamine into vesicular compartment for subsequent neurotransmitter release. The combined roles of DAT and VMAT2 are important for synaptic vesicle recycling. We measured the levels of DAT and VMAT2 after finding defects in synaptic vesicle recycling. Results of Western blot method in vivo and in vitro revealed the reduced expressions of two transporters occurring in MPTP/MPP^+ damaged groups (Fig. 7), suggesting defects in synaptic vesicle recycling and neurotransmitter release. However, PA treatment delayed the drop of DAT and VMAT2 ($p < 0.001$). For VMAT2, the protection was only significant at a higher concentration of PA ($p < 0.05$).

3.5. PA blocks PD-induced increases in calcium levels

Calcium influx triggers neurotransmitter release. Aberrant calcium accumulation is also thought to affect synaptic vesicle recycling (Verma et al., 2014). Here, we used a dye, Fura-2 AM, to quantify cytosol calcium concentration (Yun et al., 2018). In our study, calcium levels increased by approximately 50–60% in mice exposed to MPTP. The same increase also occurred in MPP^+-damaged neurons in vitro (Fig. 8). As a potent bivalent metal ions chelator, PA treatment significantly reduced the calcium levels in cytosol.

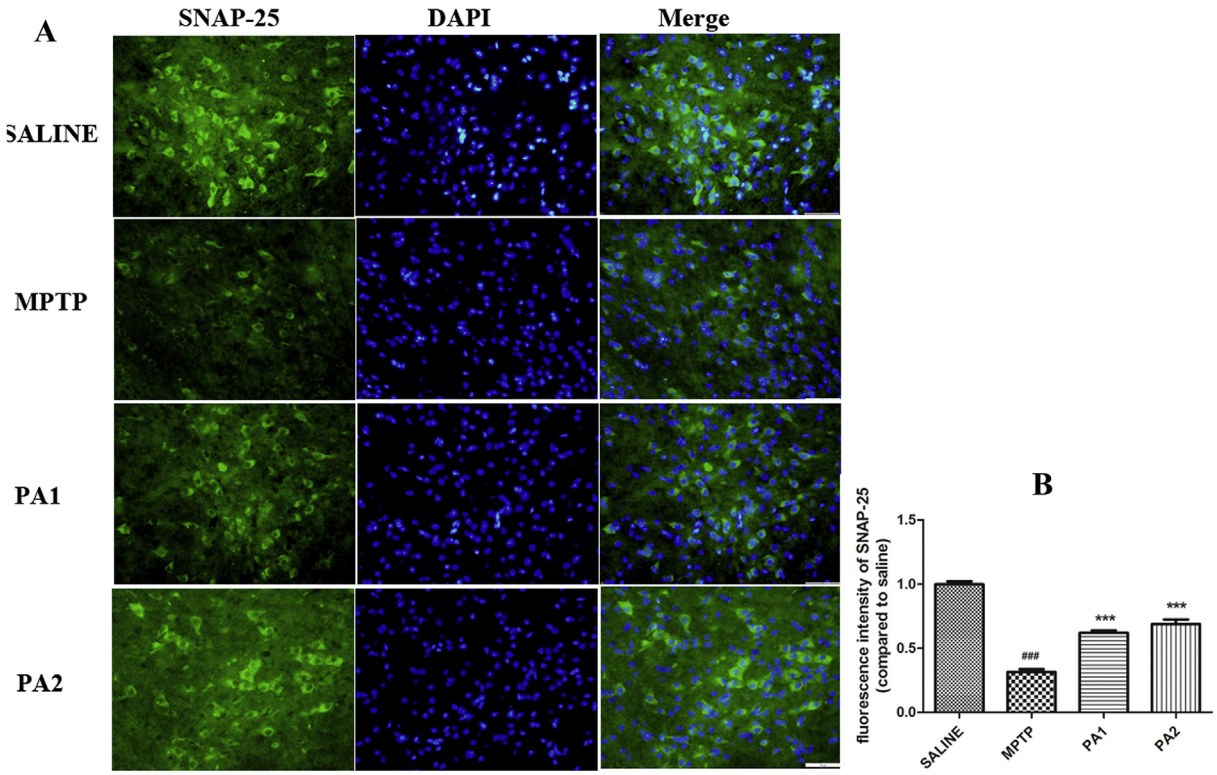

Fig. 5. SNAP-25 expression as detected using immunofluorescence. (A) SNAP-25 expression in the nigrostriatal tissues of mouse brains was measured by immunofluorescent staining. Representative confocal images comparing the expression and distribution of SNAP-25 between groups. Scale bar = 30 μ m. (B) The ratios of fluorescence intensity were compared between groups relative to saline. Data are expressed as mean ± SEM. $^{###}p < 0.001$ compared to SALINE, $^{**}p < 0.01$ compared to MPTP, $^{***}p < 0.001$ compared to MPTP. n = 6.

3.6. PA affected the expression of the Wnt-catenin pathway in PD models

Recent research indicated that the Wnt-catenin pathway, including GSK-3β, regulated the number of synapse vesicle in aged brain tissue (Inestrosa et al., 2010). With calcium influx, upregulation of GSK-3β affected synaptic vesicle recycling in cultured neurons. Here, we measured expressions of GSK-3β and β-catenin using western blotting method. Results revealed that upregulation of GSK-3β accompanied by downregulation of β-catenin when neurons exposed to MPP^+ or MPTP (Fig. 9). PA treatment inhibited the upregulation of GSK-3β and rescued the level of β-catenin ($p < 0.001$).

4. Discussion

MPTP treatment is widely used to induce neural degeneration for PD mice model. Mechanism of its selectivity in targeting the dopaminergic neurons of the substantia nigra lies in several pathways. One of the neurotoxic effects of MPTP or MPP^+ is disrupted dopamine homeostasis (St-Amour et al., 2012). The cytosolic dopamine pool is altered after neurons are treated with MPP^+. In our study, behavioral deficits and reduced dopamine release occurred in MPTP-treated mice, which suggested disturbances in synaptic vesicle recycling.

Abnormalities in synaptic vesicle recycling of presynaptic terminals occur prior to dopaminergic neuron death. To evaluate the synaptic vesicle recycling, we observed presynaptic vesicles at nerve terminals and dopamine exocytosis by using electron microscopy and fluorescent dye FM1-43, respectively. Abnormal α-synuclein is known to accumulate at presynaptic terminal and disturb synaptic vesicle recycling (Garcia et al., 2010). Synaptic failure is thought to be the pathology of degenerative diseases (Garcia et al., 2010; Overk et al., 2014). In our experiments, synaptic vesicle deficiencies were observed in the MPTP or MPP^+-damaged groups. Indeed, the number of synaptic vesicles became less, which caused defects in synaptic vesicle recycling. Some vesicles exhibited defective vesical structures. Results in vitro showed dopamine exocytosis decreased exposed to MPP^+. These results were consistent with the defects in dopamine release (Williams et al., 2016).

We measured levels of DAT and VMAT2 to determine the mechanism underlying disrupted presynaptic vesicle recycling. As a transporter, DAT carries dopamine from the presynaptic cleft into the cytosol; it also transports MPP^+ from the extracellular space to the cytosol (Richter et al., 2017). Another carrier, VMAT2, transports dopamine from the cytosol into vesicles. Thus, expressions of DAT and VMAT2 are closely related to dopamine homeostasis in neurons. In this study, we observed that MPTP/MPP^+ exposure reduced the levels of DAT and VMAT2. DAT is responsible for accumulating dopamine into the cytosol of neurons for neurotransmitter recycling. VMAT2 transports dopamine into vesicles for subsequent neurotransmitter exocytosis (Cliburn et al., 2017). Accordingly, deficiencies in expressions of DAT and VMAT2 blocked synaptic vesicle recycling and disrupted dopamine release (Lohr et al., 2017).

Previous studies have reported that GSK-3β is involved in synaptogenesis and presynaptic vesicle recycling. The Wnt pathway, including GSK-3β, is known to regulate the number of synaptic vesicles and the size of mature neurons (Hu et al., 2014; Libro et al., 2016). Upregulation of GSK-3β markedly limits presynaptic neurotransmitter release and synapse vesicle protein expression (Zhu et al., 2010). But the mechanism remains unclear. In presynaptic terminals, calcium influx contributed to the formation of a complex which regulated the reserve pool of synaptic vesicles and neurotransmitter release (Libro et al., 2016). The complex included GSK-3β and other proteins. In PD models, increased GSK-3β expression was observed and more β-catenin released from the complexes. Calcium levels were also measured in the study (Singh et al., 2016). When calcium influx entered into the cytosol to trigger the neurotransmitter release, the complexes binding with

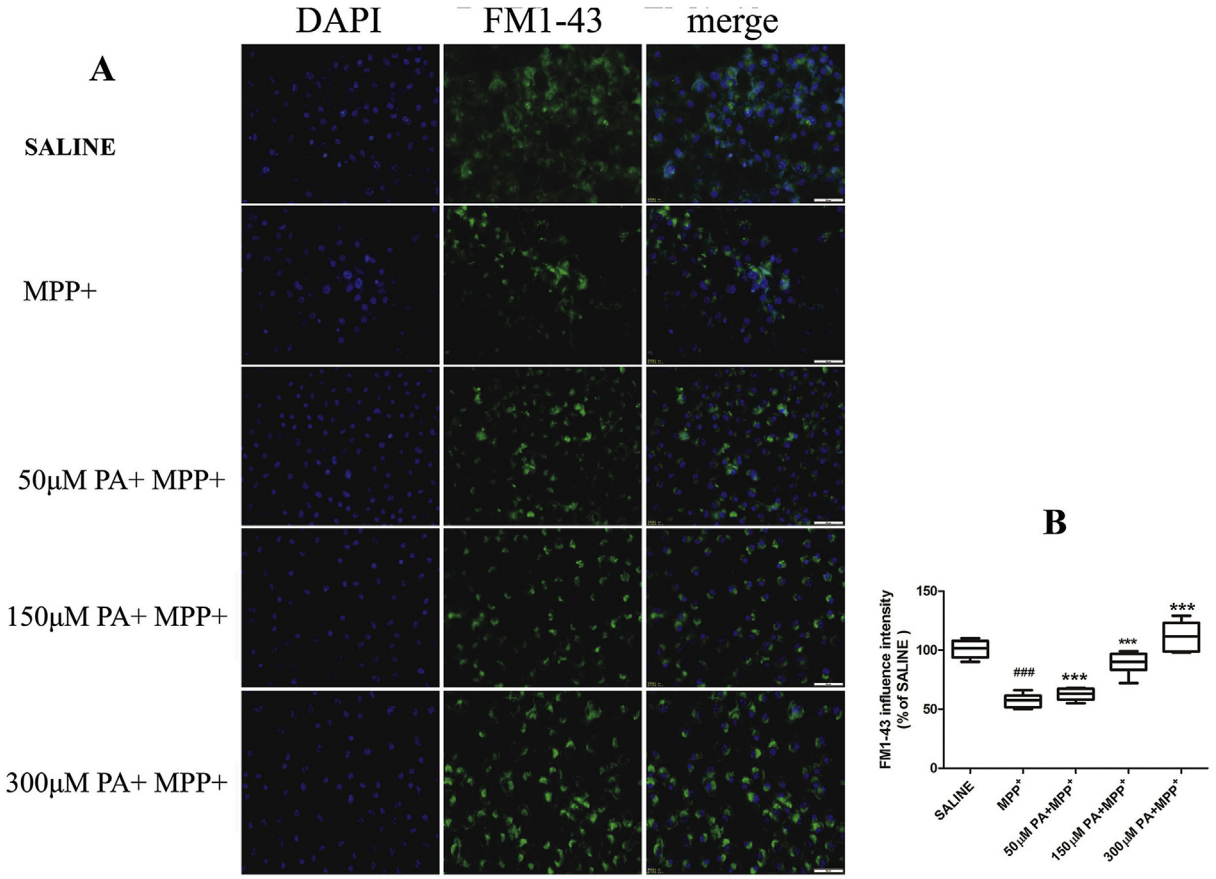

Fig. 6. PA increases synaptic vesicle recycling in MPP^+-induced SH-SY5Y neurons. (A) Synaptic vesicle retention after K+ stimulation was visualized by immunofluorescent staining with FM1-43 to stain synaptic vesicles. (B) Immunofluorescent intensities of synaptic vesicles in groups were compared to the saline group. Ratios were compared between groups. Data are expressed as mean ± SEM. $^{###}p < 0.001$ compared to SALINE, $^{**}p < 0.01$ compared to MPTP, $^{***}p < 0.001$ compared to MPTP. Scale bar = 20 μ m. n = 6.

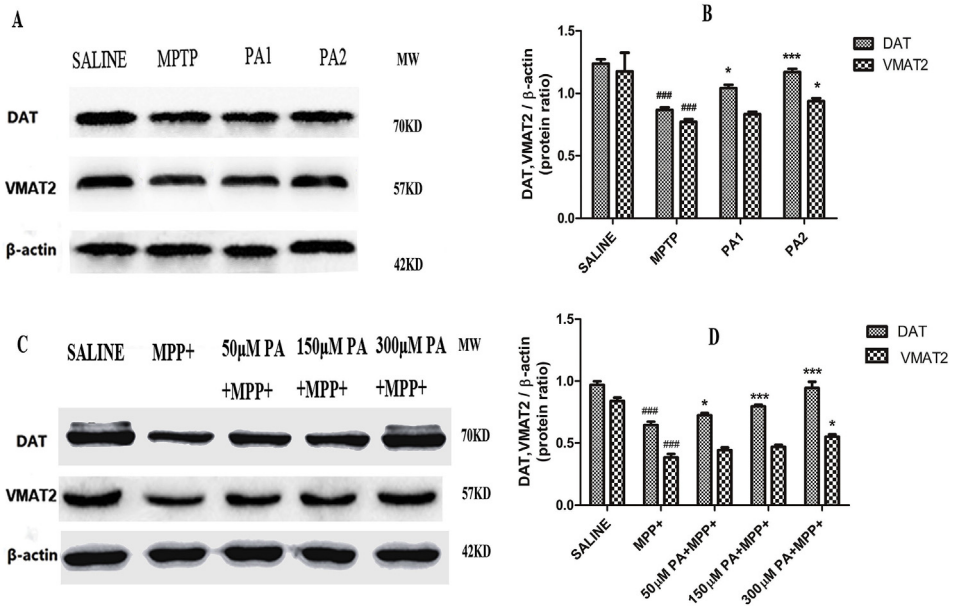

Fig. 7. PA rescues the decreased expression of DAT and VMAT2 in PD models. (A) Expressions of DAT and VMAT2 in MPTP-induced mice were observed using western blotting. (B) Values were compared among groups. (C) Expressions of DAT and VMAT2 in MPP^+-damaged cells were measured via western blotting. Values were compared between groups. Data are expressed as mean ± SEM. $^{###}p < 0.001$ compared to SALINE, $^{*}p < 0.05$ compared to MPTP. $^{**}p < 0.01$ compared to MPTP, $^{***}p < 0.001$ compared to MPTP. n = 6.

GSK-3β were involved in regulating synaptic vesicle recycling (Verma et al., 2014). It was also reported that abnormal increase in cytosolic calcium level was associated with disturbances in synaptic vesicle recycling (Choi et al., 2015).

PA is a naturally occurring compound which exists in animal and plant cells. Previously, our research showed that in PD models, PA conferred neuroprotection on dopamine neurons, inhibited apoptosis of dopaminergic neurons, and exhibited anti-inflammatory effects (Lv et al., 2015; Zhang et al., 2016b). Furthermore, PA was also found to regulate neurotransmitter release in neurons by modulating calcium-

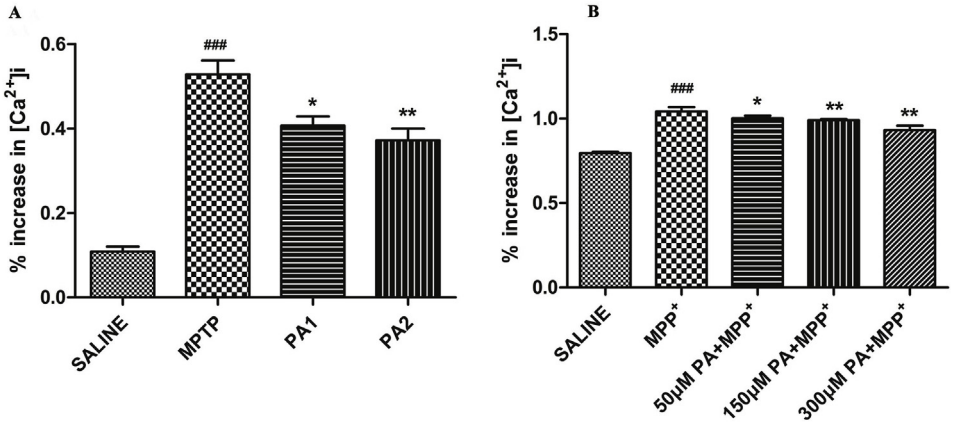

Fig. 8. PA inhibits the PD-induced calcium increase in mice and cell models. Fura-2 was used to assess cytosolic calcium levels. (A) Levels of $[Ca^{2+}]i$ in the different mouse groups are shown. (B) Levels of $[Ca^{2+}]i$ in SH-SY5Y cells. Data are expressed as mean ± SEM. $^{###}p < 0.001$ compared to SALINE, $^{*}p < 0.05$ compared to MPTP, $^{**}p < 0.01$ compared to MPTP, $^{***}p < 0.001$ compared to MPTP. n = 6.

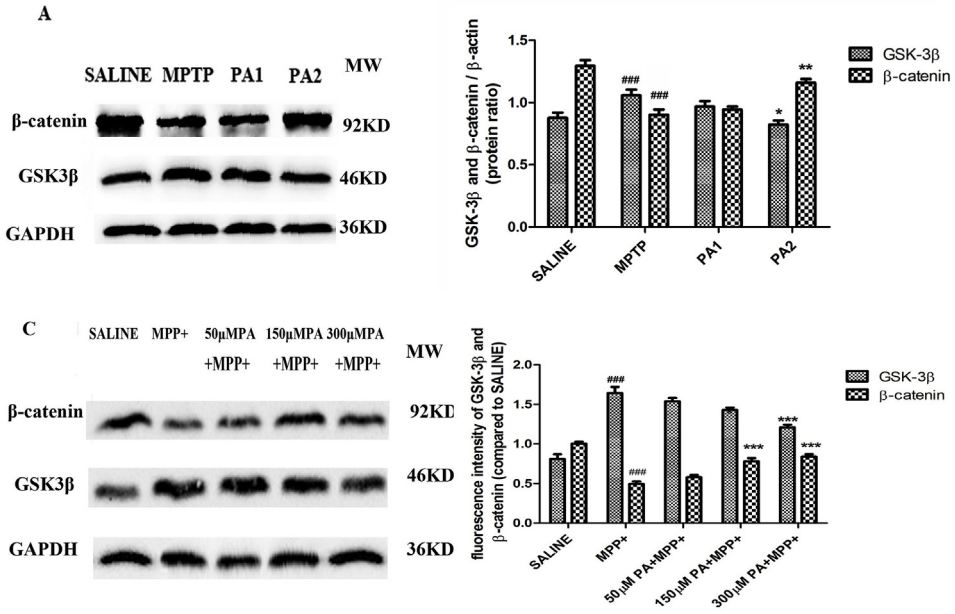

Fig. 9. PA altered the PD-induced changes in the Wnt-catenin pathway. Expression of GSK-3β and β–catenin in mice and cells was measured via western blotting and displayed in (A) and (C), respectively. Ratios of intensities of GSK-3β or β–catenin to the saline group are shown. Values in mice and cells are shown in (B) and (D), respectively. n = 6. Data are expressed as mean ± SEM. $^{###}p < 0.001$ compared to SALINE, $^{*}p < 0.05$ compared to MPTP, $^{**}p < 0.01$ compared to MPTP, $^{***}p < 0.001$ compared to MPTP.

induced synaptic vesicle exocytosis (Lu et al., 2002; Yang et al., 2012). In our study, we applied PA treatment in PD mice and cultured cells to evaluate its role on synaptic vesicle recycling. The results indicated that PA protected SH-SY5Y cells against MPP^+ damage in a dose-dependent manner. This protective effect of PA was also seen in TH + neurons in the subtantia nigra of MPTP-induced PD mice. We also observed motor defect and loss in dopamine release in the MPTP-damaged group were attenuated by PA treatment.

Movement problems arise from ongoing loss of dopamine. Thus, reduced release of this catecholamine underlies the onset of movement imbalance symptoms. Synaptic vesicle recycling includes neurotransmitter uptake and storage and vesicle exocytosis, endocytosis, and recycling (Vargas et al., 2014). These processes are complex, and the corresponding abnormalities are thought to be the toxic events that render neurons sensitive to stress. Pharmaceuticals that target members of this process to limit these disturbances have been suggested as therapies for PD (Berwick et al., 2012). In this study, electron microscopy and FM1-43 were applied to visualize synaptic vesicles in presynaptic terminals and neurotransmitter recycling. Results revealed that the MPTP/MPP^+-damaged groups had fewer synaptic vesicles and had disturbances in synaptic vesicle recycling. However, PA significantly attenuated the loss of synaptic vesicle and disturbances in neurotransmitter recycling. Increased level of SNAP-25, one of SNARE members, further confirmed PA's protection on synaptic vesicle number.

As an inhibitor of GSK-3β, PA also altered the level of β-catenin in Wnt-catenin pathway. Results showed reduced synaptic vesicles and disturbances in synaptic vesicle recycling were improved in PA treatment groups. When GSK-3β was upregulated, it contributed to release and degradation of β-catenin in the cytoplasm. The complex comprising GSK-3β, adenomatous polyposis coli (APC) and axis inhibition (AXIN) regulated synaptic vesicle recycling (Inestrosa et al., 2010). Previous studies indicated that GSK-3β negatively regulated synaptic vesicle recycling (Zhu et al., 2010). Thus, PA reversed the PD-induced reduction in synaptic vesicle recycling by controlling GSK-3β activation. PA also affected dopamine release by blocking the reduced expressions of DAT and VMAT2, which were involved in synaptic vesicle recycling.

Collectively, deficient synaptic vesicle recycling, which was observed in our study, was thought to be an early event preceding dopaminergic neuron death in PD. PA, a naturally occurring compound, attenuated disturbance in synaptic vesicle recycling and reduction in neurotransmitter release by inhibiting the upregulation of GSK-3β, blocking the decreases in levels of DAT and VMAT2, and acting as a calcium chelator. Thus, PA was suggested to be a promising therapeutic agent to treat early events in PD.

Authors' contributions

The work presented here was carried out in collaboration between all authors. L.P.W. and Z.Z participated in the design of the experiments, executed the HPLC analyses, analyzed the data and wrote the manuscript. L. H. participated in the design of the experiments, revised the manuscript. L.P.W. performed the animal studies, Immunofluorescent staining and electron microscopy method. Y.H.W. and F.Y.P performed cell culture and treatment studies, executed the Western blot detection. X.H.L. performed the flow cytometry experiments. M.L.X. and J.H.Z participated in animal studies and revised the manuscript. Y.C.L., T.W.P and J.L.X. analyzed the data and revised the manuscript. All authors read and approved the final version of the manuscript.

Conflict of interest

All authors read and approved the final version of the manuscript. The authors declare no conflict of interest.

Acknowledgements

The work presented here was carried out in collaboration between all authors. This work was funded by National Natural Science Foundation of China (81472542) and Qingdao Startup and Innovation Leader Talent Plan (13-CX-3, 201409-201709).

Appendix A. Supplementary data

Supplementary data to this article can be found online at https://doi.org/10.1016/j.neuint.2019.104507.

References

Avelar, A.J., Juliano, S.A., Garris, P.A., 2013. Amphetamine augments vesicular dopamine release in the dorsal and ventral striatum through different mechanisms. J. Neurochem. 125, 373–385.
Berwick, D.C., Harvey, K., 2012. The importance of Wnt signalling for neurodegeneration in Parkinson's disease. Biochem. Soc. Trans. 40, 1123–1128.
Blanco-Lezcano, L., Alberti-Amador, E., Díaz-Hung, M.L., González-Fraguela, M.E., Estupiñán-Díaz, B., Serrano-Sánchez, T., Francis-Turner, L., Jiménez-Martín, J., Vega-Hurtado, Y., Fernández-Jiménez, I., 2018. Tyrosine hydroxylase, vesicular monoamine transporter and dopamine transporter mRNA expression in nigrostriatal tissue of rats with pedunculopontine neurotoxic lesion. Behav. Sci. 8, 1–13.
Bradley, C.A., Peineau, S., Taghibiglou, C., Nicolas, C.S., Whitcomb, D.J., Bortolotto, Z.A., Kaang, B.K., Cho, K., Wang, Y.T., Collingridge, G.L., 2012. A pivotal role of GSK-3 in synaptic plasticity. Front. Mol. Neurosci. 5, 13.
Bridi, J.C., Hirth, F., 2018. Mechanisms of α-synuclein induced synaptopathy in Parkinson's disease. Front. Neurosci. 12, 80.
Chen, P., Gu, Z., Liu, W., Yan, Z., 2007. Glycogen synthase kinase 3 regulates N-methyl-D-aspartate receptor channel trafficking and function in cortical neurons. Mol. Pharmacol. 72, 40–51.
Choi, S.J., Panhelainen, A., Schmitz, Y., Larsen, K.E., Kanter, E., Wu, M., Sulzer, D., Mosharov, E.V., 2015. Changes in neuronal dopamine homeostasis following 1-methyl-4-phenylpyridinium (MPP+) exposure. J. Biol. Chem. 290, 6799–6809.
Cliburn, R.A., Dunn, A.R., Stout, K.A., Hoffman, C.A., Lohr, K.M., Bernstein, A.I., Winokur, E.J., Burkett, J., Schmitz, Y., Caudle, W.M., Miller, G.W., 2017. Immunochemical localization of vesicular monoamine transporter 2 (VMAT2) in mouse brain. J. Chem. Neuroanat. 83–84, 82–90.
Diao, H.L., Xue, Y., Han, X.H., Wang, S.Y., Liu, C., Chen, W.F., Chen, L., 2017. Adenosine A2A receptor modulates the activity of globus pallidus neurons in rats. Front. Physiol. 7, 897.
Garcia-Reitböck, P., Anichtchik, O., Bellucci, A., Iovino, M., Ballini, C., Fineberg, E., Ghetti, B., Della, Corte L., Spano, P., Tofaris, G.K., Goedert, M., Spillantini, M.G., 2010. SNARE protein redistribution and synaptic failure in a transgenic mouse model of Parkinson's disease. Brain 133, 2032–2044.
Grases, F., Simonet, B.M., Prieto, R.M., March, J.G., 2001. Variation of InsP(4),InsP(5) and InsP(6) levels in tissues and biological fluids depending on dietary phytate. J. Nutr. Biochem. 12, 595–601.
Hu, F., Xu, L., Liu, Z.H., Ge, M.M., Ruan, D.Y., Wang, H.L., 2014. Developmental lead exposure alters synaptogenesis through inhibiting canonical Wnt pathway in vivo and in vitro. PLoS One 9, e101894.
Inestrosa, N.C., Arenas, E., 2010. Emerging roles of Wnts in the adult nervous system. Nat. Rev. Neurosci. 11, 77–86.
Jensen, K.L., Runegaard, A.H., Weikop, P., Gether, U., Rickhag, M., 2017. Assessment of dopaminergic homeostasis in mice by use of high-performance liquid chromatography analysis and synaptosomal dopamine uptake. J. Vis. Exp. 21, 127.
Jia, F., Song, N., Wang, W., Du, X., Chi, Y., Jiang, H., 2018. High dietary iron supplement induces the nigrostriatal dopaminergic neurons lesion in transgenic mice expressing mutant A53T human alpha-synuclein. Front. Aging Neurosci. 10, 97.
Leikas, J.V., Kohtala, S., Theilmann, W., Jalkanen, A.J., Forsberg, M.M., Rantamäki, T., 2017. Brief isoflurane anesthesia regulates striatal AKT-GSK3β signaling and ameliorates motor deficits in a rat model of early-stage Parkinson's disease. J. Neurochem. 142, 456–463.
Libro, R., Bramanti, P., Mazzon, E., 2016. The role of the Wnt canonical signaling in neurodegenerative diseases. Life Sci. 1, 78–88.
Lohr, K.M., Bernstein, A.I., Stout, K.A., Dunn, A.R., Lazo, C.R., Alter, S.P., Wang, M., Li, Y., Fan, X., Hess, E.J., Yi, H., Vecchio, L.M., Goldstein, D.S., Guillot, T.S., Salahpour, A., Miller, G.W., 2014. Increased vesicular monoamine transporter enhances dopamine release and opposes Parkinson disease-related neurodegeneration in vivo. Proc. Natl. Acad. Sci. U.S.A. 8, 9977–9982.
Lohr, K.M., Masoud, S.T., Salahpour, A., Miller, G.W., 2017. Membrane transporters as mediators of synaptic dopamine dynamics: implications for disease. Eur. J. Neurosci. 45, 20–33.
Lu, Y.J., He, Y., Sui, S.F., 2002. Inositol hexakisphosphate (InsP6) can weaken the Ca(2+)-dependent membrane binding of C2AB domain of synaptotagmin I. FEBS Lett. 11, 22–26.
Lv, Y., Zhang, Z., Hou, L., Zhang, L., Zhang, J., Wang, Y., Liu, C., Xu, P., Liu, L., Gai, X., Lu, T., 2015. Phytic acid attenuates inflammatory responses and the levels of NF-κB and p-ERK in MPTP-induced Parkinson's disease model of mice. Neurosci. Lett. 15, 132–136.
Ma, Z.G., Wang, G.L., Cui, L., Wang, Q.M., 2015. Myricetin attenuates depressant-like behavior in mice subjected to repeated restraint stress. Int. J. Mol. Sci. 6, 28377–28385.
Mackenzie, K.D., Lumsden, A.L., Guo, F., Duffield, M.D., Chataway, T., Lim, Y., Zhou, X.F., Keating, D.J., 2016. Huntingtin-associated protein-1 is a synapsin I-binding protein regulating synaptic vesicle exocytosis and synapsin I trafficking. J. Neurochem. 138, 710–721.
Marland, J.R., Hasel, P., Bonnycastle, K., Cousin, M.A., 2016. Mitochondrial calcium uptake modulates synaptic vesicle endocytosis in central nerve terminals. J. Biol. Chem. 29, 2080–2086.
Overk, C.R., Masliah, E., 2014. Pathogenesis of synaptic degeneration in Alzheimer's disease and Lewy body disease. Biochem. Pharmacol. 15, 508–516.
Richter, F., Gabby, L., McDowell, K.A., Mulligan, C.K., De, LaRosaK., Sioshansi, P.C., Mortazavi, F., Cely, I., Ackerson, L.C., Tsan, L., Murphy, N.P., Maidment, N.T., Chesselet, M.F., 2017. Effects of decreased dopamine transporter levels on nigrostriatal neurons and paraquat/maneb toxicity in mice. Neurobiol. Aging 51, 54–66.
Rockenstein, E., Nuber, S., Overk, C.R., Ubhi, K., Mante, M., Patrick, C., Adame, A., Trejo-Morales, M., Gerez, J., Picotti, P., Jensen, P.H., Campioni, S., Riek, R., Winkler, J., Gage, F.H., Winner, B., Masliah, E., 2014. Accumulation of oligomer-prone α-synuclein exacerbates synaptic and neuronal degeneration in vivo. Brain 137, 1496–1513.
Singh, S., Mishra, A., Shukla, S., 2016. ALCAR exerts neuroprotective and pro-neurogenic effects by inhibition of glial activation and oxidative stress via activation of the wnt/β-catenin signaling in parkinsonian rats. Mol. Neurobiol. 53, 4286–4301.
St-Amour, I., Bousquet, M., Paré, I., Drouin-Ouellet, J., Cicchetti, F., Bazin, R., Calon, F., 2012. Impact of intravenous immunoglobulin on the dopaminergic system and immune response in the acute MPTP mouse model of Parkinson's disease. J. Neuroinflammation 9, 234.
Vargas, K.J., Makani, S., Davis, T., Westphal, C.H., Castillo, P.E., Chandra, S.S., 2014. Synucleins regulate the kinetics of synaptic vesicle endocytosis. J. Neurosci. 9, 9364–9376.
Verma, M., Steer, E.K., Chu, C.T., 2014. ERKed by LRRK2: a cell biological perspective on hereditary and sporadic Parkinson's disease. Biochim. Biophys. Acta 1842, 1273–1281.
Wang, Q., Qian, L., Chen, S.H., Chu, C.H., Wilson, B., Oyarzabal, E., Ali, S., Robinson, B., Rao, D., Hong, J.S., 2015. Post-treatment with an ultra-low dose of NADPH oxidase inhibitor diphenyleneiodonium attenuates disease progression in multiple Parkinson's disease models. Brain 138, 1247–1262.
Wang, Q.M., Xu, Y.Y., Liu, S., Ma, Z.G., 2017. Isradipine attenuates MPTP-induced dopamine neuron degeneration by inhibiting up-regulation of L-type calcium channels and iron accumulation in the substantia nigra of mice. Oncotarget 18, 47284–47295.
Williams, R.S., Bate, C., 2016. An in vitro model for synaptic loss in neurodegenerative diseases suggests a neuroprotective role for valproic acid via inhibition of cPLA2 dependent signalling. Neuropharmacology 101, 566–575.
Yang, S.N., Shi, Y., Yang, G., Li, Y., Yu, L., Shin, O.H., Bacaj, T., Südhof, T.C., Yu, J., Berggren, P.O., 2012. Inositol hexakisphosphate suppresses excitatory neurotransmission via synaptotagmin-1 C2B domain in the hippocampal neuron. Proc. Natl. Acad. Sci. U.S.A. 24, 12183–12188.
Yun, S.P., Kim, D., Kim, S., Kim, S., Karuppagounder, S.S., Kwon, S.H., Lee, S., Kam, T.I., Lee, S., Ham, S., Park, J.H., Dawson, V.L., Dawson, T.M., Lee, Y., Ko, H.S., 2018. α-Synuclein accumulation and GBA deficiency due to L444P GBA mutation contributes to MPTP-induced parkinsonism. Mol. Neurodegener. 8, 1.
Zhang, L., Cen, L., Qu, S., Wei, L., Mo, M., Feng, J., Sun, C., Xiao, Y., Luo, Q., Li, S., Yang, X., Xu, P., 2016a. Enhancing beta-catenin activity via GSK3beta inhibition protects PC12 cells against rotenone toxicity through Nurr1 induction. PLoS One 5, e0152931.
Zhang, Z., Hou, L., Li, X., Ju, C., Zhang, J., Li, X., Wang, X., Liu, C., Lv, Y., Wang, Y., 2016b. Neuroprotection of inositol hexaphosphate and changes of mitochondrion mediated apoptotic pathway and α-synuclein aggregation in 6-OHDA induced Parkinson's disease cell model. Brain Res. 15, 87–95.
Zhu, L.Q., Liu, D., Hu, J., Cheng, J., Wang, S.H., Wang, Q., Wang, F., Chen, J.G., Wang, J.Z., 2010. GSK-3 beta inhibits presynaptic vesicle exocytosis by phosphorylating P/Q-type calcium channel and interrupting SNARE complex formation. J. Neurosci. 10, 3624–3633.